Pei-Wei Han, Hai-Juan Wang* and Shao-Jun Chu

The Calculation for Saturated Solubility of Oxygen in Mn–Si Melts Equilibrated with MnO–SiO_2 Slags

DOI 10.1515/htmp-2015-0136
Received June 10, 2015; accepted November 24, 2015

Abstract: The MnO–SiO_2 slag in equilibrium with Mn–Si melts with a Si molar ratio between 0.1 and 0.3 at 1,700 K was a single liquid phase. However, it was liquid phase saturated with solid MnO or solid SiO_2 in the case of X_{Si} less than 0.1 or greater than 0.3, respectively. Based on a subregular solution model, the calculated saturated solubility of oxygen in Mn–Si melts was 0.0236 mass % in pure manganese at 1,700 K and increased with the increasing silicon in the range of X_{Si} from 0.1 to 0.3. However, the saturated solubility of oxygen decreases as the silicon exceeded 0.3, and the minimum solubility was 0.0041 mass % in pure silicon at 1,700 K. The results could be used to predict the compositions of endogenous oxide inclusions and evaluate the cleanliness of manganese ferroalloy.

Keywords: Mn–Si melts, oxide phase, saturated solubility of oxygen, oxide inclusions, cleanliness

Introduction

Attention has been attracted to the study of ferroalloy cleanliness as a consequence of the development of clean steels [1–3]. However, the impurity elements and nonmetallic inclusions and their associated effects on the quality of steel are rarely studied in detail [4–10].

Manganese ferroalloys are widely used as alloying or deoxidizing materials in steelmaking processes, and unavoidable incorporate inclusions into the steel. The amount, size and composition of inclusions in steel were affected by that in manganese ferroalloy to some extent. In laboratory trials, more inclusions were expected in steel if the ferromanganese contained more impurities [9]. But in plant trials, ferromanganese grades only had a temporary influence on the content and compositions of micro-inclusions in steel [10]. The steel quality was affected by the inclusions in ferromanganese, especially when it is added as a final adjustment immediately before casting.

The total oxygen content and inclusions in silicomanganese ferroalloy (SiMn) as well as in low carbon ferromanganese (LCFeMn) and medium carbon ferromanganese (MCFeMn) produced from different processes have been studied in Refs [2, 11–13]. The results showed that the silicon content and production process have significant influences on the compositions and types of inclusions in ferromanganese alloys. MnO is the predominant nonmetallic inclusion in LCFeMn and MCFeMn produced through the oxygen refining method, while the MnO–SiO_2-type complex inclusions and MnS inclusions are the secondly dominated inclusions [11]. However, the MnO–SiO_2-type complex inclusions predominate in MCFeMn and LCFeMn produced by the shaking ladle-electro-silicothermic process [13]. The complex inclusion is attributed to tephroite ($2MnO{\cdot}SiO_2$), and minor insoluble SiO_2 inclusions are also left in the electrochemical etching [2]. In SiMn, the dominated inclusions include silica, silicate-containing manganese oxide and iron oxides, which are determined by electrochemical etching of bulk samples in an aqueous solution [13]. However, the main inclusions were rare earth metal (REM) oxides with some amounts of Si and Mn in SiMn by electrolytic extraction using nonaqueous solution as an electrolyte [14]. Although previous study provided useful information about the chemical composition and morphology of inclusions in manganese ferroalloys, the relationship between the saturated solubility of oxygen and the silicon content in Mn–Si melt is not clear, although this relationship is significantly important for steel quality. However, it is possible to calculate the saturated solubility of oxygen in Mn–Si melts based on the work about the thermodynamics of oxygen solutions in liquid manganese [15–17], silicon [18, 19] and Fe–Mn melts [16, 20].

The types of oxide inclusions were related to silicon content in MCFeMn and LCFeMn, which can be taken as Mn–Si–Fe system with a Si content less than 1 mass %

***Corresponding author: Hai-Juan Wang,** Dept. of Ferrous Metallurgy, School of Metallurgical and Ecological Engineering, University of Science and Technology Beijing, Beijing 100083, China, E-mail: wanghaijuan@ustb.edu.cn
Pei-Wei Han, Shao-Jun Chu, Dept. of Ferrous Metallurgy, School of Metallurgical and Ecological Engineering, University of Science and Technology Beijing, Beijing 100083, China

and it is studied using a simplified Mn–Si system. The purpose of this work is to calculate the thermodynamic data and study the relationship of the oxide inclusions with the saturated solubility of oxygen, which is a function of the silicon content in the Mn–Si melt. Then the research could be expanded to MCFeMn and LCFeMn and SiMn to provide theoretical support for the development of secondary refining process of manganese ferroalloys and material selections for the steel quality control.

Thermodynamic models and parameters

Thermodynamic model

A subregular solution model proposed by Hajra et al. [21] can be applied to interpret the thermodynamic behaviors of solutes in binary metallic solutions. Assuming that the component 2 is taken as an interstitial solute in the metal components 1 and 3 in the ternary system 1–2–3, the activity coefficient of infinite dilution $\ln \gamma^{\circ}_{2(1-3)}$ and self-interaction parameter of component 2 $\varepsilon^{2}_{2(1-3)}$ can be expressed as

$$\ln \gamma^{\circ}_{2(1-3)} = X_1 \ln \gamma^{\circ}_{2(1)} + X_3 \ln \gamma^{\circ}_{2(3)} + X_1X_3[X_3(\ln \gamma^{\circ}_{2(1)} - \ln \gamma^{\circ}_{2(3)} + \varepsilon^{3}_{2(1)}) + X_1(\ln \gamma^{\circ}_{2(3)} - \ln \gamma^{\circ}_{2(1)} + \varepsilon^{1}_{2(3)})] \quad (1)$$

$$\varepsilon^{2}_{2(1-3)} = X_1\varepsilon^{2}_{2(1)} + X_3\varepsilon^{2}_{2(3)} + X_1X_3\left[\frac{1}{2}X_3\phi_1 - \frac{\phi_2}{1-X_1X_3}\right] \quad (2)$$

where $\gamma^{\circ}_{2(1)}$ and $\gamma^{\circ}_{2(3)}$ are the activity coefficients of component 2 in infinite dilution in solvents 1 and 3, respectively; $\varepsilon^{3}_{2(1)}$ is the first-order interaction parameter of component 3 on component 2 in solvent 1; $\varepsilon^{1}_{2(3)}$ is the first-order interaction parameter of component 1 on component 2 in solvent 3; $\varepsilon^{2}_{2(1)}$ and $\varepsilon^{2}_{2(3)}$ are the self-interaction parameters of component 2 in solvents 1 and 3, respectively; ϕ_1 and ϕ_2 are the higher order interaction terms that are treated as zero in most cases [20].

The values of $\ln \gamma^{\circ}_{O}$ and ε^{O}_{O} calculated from the above model are in agreement with the experimental values well for the systems of Pb–O–Sb, Pb–O–Bi and Pb–O–Cu [21]. Similarly, it can also be used to interpret $\ln \gamma^{\circ}_{S}$ and $\ln \gamma^{\circ}_{O}$ in Cu–S–Sb system [22] and Fe–O–Si system [23] and predict the saturated solubility of oxygen in Fe–Mn melts [20] and the deoxidation equilibrium of silicon and manganese in Fe–Ni melts [24].

Since the Mn–Si melts can be treated as a subregular solution [25], the model is adopted to calculate the saturated solubility of oxygen in Mn–Si melts in the present study. Assuming that manganese and silicon are the solvents and oxygen is the solute for the Mn–O–Si system, the activity coefficient of oxygen, $\gamma^{\circ}_{O(Mn-Si)}$, in infinite dilution range and the self-interaction parameter of oxygen $\varepsilon^{O}_{O(Mn-Si)}$ are expressed as

$$\ln \gamma^{\circ}_{O(Mn-Si)} = X_{Mn} \ln \gamma^{\circ}_{O(Mn)} + X_{Si} \ln \gamma^{\circ}_{O(Si)} + X_{Mn}X_{Si}[X_{Mn}(\gamma^{\circ}_{O(Mn)} - \ln \gamma^{\circ}_{O(Si)} + \varepsilon^{Si}_{O(Mn)}) + X_{Si}(\ln \gamma^{\circ}_{O(Si)} - \ln \gamma^{\circ}_{O(Mn)} + \varepsilon^{Mn}_{O(Si)})] \quad (3)$$

$$\varepsilon^{O}_{O(Mn-Si)} = X_{Mn}\varepsilon^{O}_{O(Mn)} + X_{Si}\varepsilon^{O}_{O(Si)} \quad (4)$$

Saturated solubility of oxygen in Mn–Si melts can be calculated by one of the reactions listed later, respectively. Equation (5) is suited for that the oxide phase is liquid phase saturated with solid SiO_2, while eq. (6) is applied in the situation where the oxide phase is liquid phase saturated with solid MnO:

$$(SiO_2) = [Si]_{(Mn-Si)} + 2[O]_{(Mn-Si),1\%} \quad (5)$$

$$(MnO) = [Mn]_{(Mn-Si)} + [O]_{(Mn-Si),1\%} \quad (6)$$

Activities of manganese and silicon in Mn–Si melts

Activities of manganese in Mn–Si melts are measured by transportation technique [25, 26], torsion-effusion method [27, 28] and electromagnetic force (EMF) method [29]. The activities of silicon are derived from the measured manganese activity and the Gibbs–Duhem equation or obtained from the equilibrium between Mn–Si melts and MnO-containing slags [30–32]. The results reported by different authors are consistent. Activities of manganese and silicon in Mn–Si melts at 1,700 K reported by Ahmad and Pratt [27] are selected for the present calculations and are listed in Table 1.

Thermodynamics of oxygen in manganese melt

The saturated solubility of oxygen in manganese differs greatly with each other in different works [14, 16, 17]. Thermodynamics of oxygen in manganese melt are studied following the method used by Pivovarov et al. [20].

Table 1: Compositions of MnO–SiO_2 slags in equilibrium with Mn–Si melts at 1,700 K.

Mn–Si melts				MnO–SiO_2 slags				
x_{Si}	[% Si]	a_{Mn}[27]	a_{Si}[27]	a_{MnO}	a_{SiO_2}	(MnO) (mass %)	(SiO_2) (mass %)	Phase
0	0	1	0	1	0	100	0	Solid MnO
0.1	5.38	0.8645	6.7×10^{-5}	0.8950	0.0484	74.64	25.36	Liquid phase
0.2	11.33	0.5829	0.0006	0.4275	0.2201	66.58	33.42	
0.3	17.97	0.2852	0.0052	0.1491	0.9564	52.65	47.35	
0.4	25.42	0.0929	0.0408	0.144	1	–	–	Liquid phase
0.5	33.83	0.0305	0.1656			–	–	saturated
0.6	43.40	0.0117	0.3613			–	–	with solid
0.7	54.40	0.0049	0.5830			–	–	SiO_2
0.8	67.16	0.0023	0.7520			–	–	
0.9	82.15	0.0008	0.8934			–	–	
1	100	0	1	0	1	0	100	Solid SiO_2

The saturated solubility of oxygen in manganese could be calculated through the following equations:

$$\mathrm{MnO(s)} = \mathrm{Mn(l)} + [\mathrm{O}]_{(\mathrm{Mn}),1\%} \tag{7}$$

$$\Delta G_7^\circ = 104,586 - 30.27T \quad \mathrm{J/mol}[20] \tag{8}$$

$$K_7 = f_{\mathrm{O}}[\%\mathrm{O}] \tag{9}$$

The activity of Mn could be regarded as unity, and thus K_7 almost is equal to $f_{\mathrm{O}}[\%\mathrm{O}]$. As [% O] approaches to zero, the value of f_{O} approaches to unity due to $\lg f_{\mathrm{O}} = e_{\mathrm{O}}^{\mathrm{O}}[\%\mathrm{O}]$, and K_7 is approximately equal to [% O]. Hence, the value 0.0095 of $[\%\mathrm{O}]_{(\mathrm{Mn})}^{\mathrm{sat}}$ [16] at 1,515 K is reliable. Thus, it is possible to calculate the interaction coefficient of activity $e_{\mathrm{O(Mn)}}^{\mathrm{O}}$ at 1,515 K as shown in eq. (10):

$$e_{\mathrm{O(Mn)}}^{\mathrm{O}}(1,515\ \mathrm{K}) = -(\lg K_7 - \lg[\%\mathrm{O}]_{(\mathrm{Mn})}) \Big/ [\%\mathrm{O}]_{(\mathrm{Mn})} = -0.274 \tag{10}$$

Since the temperature of interest is higher than 1,515 K, it is desirable to assume a temperature-dependent interaction coefficient based on the regular solution [33]. The relationship can be written as [34]

$$T_1 e_j^i(T_1) = T_2 e_j^i(T_2) \tag{11}$$

For regular solution, there is

$$RT\ln\gamma_i = b(1-N_i)^2 \tag{12}$$

where b is a constant which is independent of temperature.

γ_i could be also represented as

$$\gamma_i = \gamma_i^0 f_i \tag{13}$$

Substituting γ_i in eq. (12) using eq. (13), the following equation was obtained:

$$(RT\ln\gamma_i^0 + RT\ln f_i)_{T_1} = (RT\ln\gamma_i^0 + RT\ln f_i)_{T_2} \tag{14}$$

With partial differentiation, the following is obtained:

$$\left[\frac{\partial(RT\ln\gamma_i^0 + RT\ln f_i)}{\partial(\%\,j)}\right]_{T_1} = \left[\frac{\partial(RT\ln\gamma_i^0 + RT\ln f_i)}{\partial(\%\,j)}\right]_{T_2} \tag{15}$$

$$\left[2.303RT\frac{\partial\lg f_i}{\partial(\%\,j)}\right]_{T_1} = \left[2.303RT\frac{\partial\lg f_i}{\partial(\%\,j)}\right]_{T_2} \tag{16}$$

Equation (11) was obtained from eq. (16).

Thus, the value of $e_{\mathrm{O(Mn)}}^{\mathrm{O}}$ at 1,700 K is −0.244, and $[\%\mathrm{O}]_{(\mathrm{Mn})}^{\mathrm{sat}}(1700\ \mathrm{K}) = 0.0236$.

The reaction of oxygen dissolving in liquid manganese can be expressed as

$$1/2\mathrm{O_2(g)} = [\mathrm{O}]_{(\mathrm{Mn}),1\%} \tag{17}$$

$$\Delta G_{17}^\circ = -302,287 + 57.78T \quad \mathrm{J/mol} \qquad [20] \tag{18}$$

At 1,700 K, the value of $\gamma_{\mathrm{O}}^\circ(\mathrm{Mn})$ is 1.56×10^{-5} due to $\Delta G_{17}^\circ = RT\ln\left[\gamma_{\mathrm{O(Mn)}}^\circ\frac{M_{\mathrm{Mn}}}{100M_{\mathrm{O}}}\right]$.

Thermodynamics of oxygen in silicon melt

Oxygen solubility in liquid silicon can be described by the following equation with the equilibrium of SiO_2:

$$\lg[\%\mathrm{O}]_{(\mathrm{Si})}^{\mathrm{sat}} = 0.332 - 4,620/-\mathrm{T} \quad (1,693-1,823\ \mathrm{K}) \quad [18] \tag{19}$$

The standard free energy change for oxygen dissolving in liquid silicon can be expressed as follows:

$$1/2\mathrm{O_2(g)} = [\mathrm{O}]_{(\mathrm{Si}),1\%} \tag{20}$$

$$\Delta G_{20}^\circ = -388,000 + 95.6T \quad \mathrm{J/mol} \quad [18] \tag{21}$$

Thus, $[\%O]^{sat}_{(Si)} = 0.0041$ at 1,700 K and the value of $\gamma^{\circ}_{O(Si)}$ is 6.72×10^{-6}.

For silicon, the reaction between metal and oxide can be written as

$$SiO_2(s) = Si(l) + 2[O]_{(Si),\,1\%} \quad (22)$$

$$\Delta G^{\circ}_{22} = -177,000 + 12.7T \quad J/mol[18] \quad (23)$$

The value of $e^{O}_{O(Si)}(1,700\ K)$ is −0.492, which is obtained through the similar method to that calculating $e^{O}_{O(Mn)}$ in the present paper.

Determination of $\varepsilon^{Si}_{O(Mn)}$ and $\varepsilon^{Mn}_{O(Si)}$

The value of $e^{Si}_{O(Mn)}$ is −0.0199 at 1,823 K [17]. The value of $e^{Si}_{O(Mn)}$ at 1,700 K is determined to be −0.0213 via eq. (11). Thus, $\varepsilon^{Si}_{O(Mn)}(1,700\ K) = -2.021$, according to the relationship shown in eq. (24) [35]:

$$e^{j}_{i} = \frac{1}{230}\left\{(\varepsilon^{j}_{i} - 1)\frac{M_1}{M_j} + 1\right\} \quad (24)$$

$\varepsilon^{Mn}_{O(Si)}$ and $e^{Mn}_{O(Si)}$ have not been reported in literatures, and they are determined based on the following principles for parameter selection. At 1,873 K, the value of $\varepsilon^{Fe}_{O(Si)}$ is -6.5 ± 2.0 according to Ref. [23], and the associated $e^{Fe}_{O(Si)}$ is -0.0123 ± 0.0045. In addition, the value of $e^{Fe}_{O(Si)}$ is −0.015 presented in Ref. [19], which is in the range obtained from Ref. [23]. Mn–Fe melts were treated as ideal solution, and it is reasonable to assume that thermodynamic behavior of Mn is similar to Fe in silicon-based melts to some extent. Thus, the value of $\varepsilon^{Mn}_{O(Si)}$ could be evaluated from $\varepsilon^{Fe}_{O(Si)}$. Considering the stronger affinity between oxygen and manganese than iron, it is reasonable to assume that $e^{Fe}_{O(Si)}$ is slightly larger than $e^{Mn}_{O(Si)}$. Thus, the minimum value of $e^{Fe}_{O(Si)} -0.0123 \pm 0.0045$, which is −0.0168 at 1,873 K is chosen for $e^{Mn}_{O(Si)}$ in the current evaluation. According to eqs (11) and (24), the values of $e^{Mn}_{O(Si)}$ and $\varepsilon^{Mn}_{O(Si)}$ at 1,700 K are −0.0185 and −9.2677, respectively.

Activities of MnO and SiO_2 in MnO–SiO_2 binary system

The methods for measuring the activity of MnO and SiO_2 in the MnO–SiO_2 melt have been discussed in Refs [36–38]. The equilibrium reactions shown in eq. (25) are established in a three-phase system, including the MnO–SiO_2 melt, atmospherical gas with a fixed ratio of oxygen and a Pt–Mn foil immersed in the melt. The activity of MnO in the melt is obtained based on the activity of Mn and the oxygen partial pressure above the Pt–Mn alloy, while the activities of SiO_2 are derived from the Gibbs–Duhem equation:

$$[Mn]_{Platinum} + 1/2O_2(g) = (MnO) \quad (25)$$

Gaskell [39] recalculated the activities of MnO and SiO_2 in the MnO–SiO_2 melt by applying the re-determined Mn activities in Pt–Mn alloy. It was found that the activities of MnO were 25 % smaller than the original values, but the activities of SiO_2 were similar to the previous ones. The data of MnO activities obtained by Rao and Gaskell [38] were also significantly lower than those obtained from the previous investigations [36, 37]. However, activities of SiO_2 are consistent.

In the present paper, the data reported by Rao and Gaskell [38] are adopted as the activities of MnO and SiO_2 at 1,700 K.

Results

Compositions of the oxide phases in equilibrium with Mn–Si melts at 1,700 K

The oxide phases in equilibrium with Mn–Si melts consist of MnO and SiO_2. The compositions of oxide phase vary as the silicon content increases in the Mn–Si melts. The equilibrium between Mn–Si melts and oxide phases could be expressed as

$$2(MnO) + [Si]_{Mn-Si} = (SiO_2) + 2[Mn]_{Mn-Si} \quad (26)$$

$$K_{26} = \frac{a^2_{Mn} a_{SiO_2}}{a_{Si} a^2_{MnO}} \quad (27)$$

The values of standard formation Gibbs free energy of MnO and SiO_2 are −257,188 J/mol [20] and −606,240 J/mol [18], respectively, at 1,700 K. Thus, the value of ΔG°_{26} and K_{26} at 1,700 K are determined to be −91,684 and 664.87 J/mol, respectively. The compositions of oxide phases in equilibrium with Mn–Si melts at 1,700 K were obtained according to eq. (27), and the results are shown in Table 1.

According to the MnO–SiO_2 binary phase diagram, the mass percent of MnO and SiO_2 in liquid phase saturated with solid MnO are 76.11 and 23.89, respectively, at 1,700 K, while they are 51.92 and 48.08 in liquid phase saturated with solid SiO_2, respectively.

Comparison between the calculated results and the phase diagram of MnO–SiO_2 binary system demonstrates that the oxide phase is liquid phase saturated with solid

MnO when the molar ratio X_{Si} is less than 0.1. However, the oxide phase becomes saturated with solid SiO_2 when X_{Si} is greater than 0.3. The single equilibrium liquid slags with Mn–Si melts only exist over the silicon content ranging from 0.1 to 0.3.

Saturated solubility of oxygen in Mn–Si melts at 1,700 K

The chemical reactions and the associated standard free energy change for dissolved oxygen in Mn–Si melts can be expressed by the following equation:

$$1/2O_2 = [O]_{(Mn-Si),1\%} \tag{28}$$

$$\Delta_{sol}G_O^\circ = RT\ln\left[\gamma_{O(Mn-Si)}^\circ \frac{M_{Mn-Si}}{100M_O}\right] \tag{29}$$

where the value of $\gamma_{O(Mn-Si)}^\circ$ is obtained by eq. (3), M_{Mn-Si} is calculated via eq. (30). The values of $\gamma_{O(Mn-Si)}^\circ$, $\Delta_{sol}G_O^\circ$ and M_{Mn-Si} are shown in Table 2:

$$M_{Mn-Si} = X_{Mn}M_{Mn} + X_{Si}M_{Si} \tag{30}$$

Equation (5) is applied when SiO_2 is the main component in the oxide phase. The standard free energy change and reaction equilibrium constant of eq. (5) are described as follows:

$$\Delta G_5^\circ = 2\Delta_{sol}G_O^\circ - \Delta_f G_{SiO_2}^\circ \tag{31}$$

$$K_5 = \frac{a_{Si}f_O^2[\%O]^2}{a_{SiO_2}} \tag{32}$$

The saturated solubility of oxygen can be obtained by applying eq. (33):

$$\lg[\%O] + e_{O(Mn-Si)}^O[\%O] + (\lg a_{Si} - \lg a_{SiO_2} - \lg K_5)/-2 = 0 \tag{33}$$

where the value of $e_{O(Mn-Si)}^O$ is obtained from eq. (34):

$$e_{O(Mn-Si)}^O = X_{Mn}e_{O(Mn)}^O + X_{Si}e_{O(Si)}^O \tag{34}$$

For the oxide slags with MnO as the predominant species, eq. (6) is adopted to calculate the saturated solubility of oxygen. The change of standard free energy and reaction equilibrium constant of eq. (6) are given in eqs (35) and (36), respectively:

$$\Delta G_6^\circ = \Delta_{sol}G_O^\circ - \Delta_f G_{MnO}^\circ \tag{35}$$

$$K_6 = \frac{a_{Mn}f_O[\%O]}{a_{MnO}} \tag{36}$$

The saturated solubility of oxygen can be obtained via eq. (37):

$$\lg[\%O] + e_{O(Mn-Si)}^O[\%O] + (\lg a_{Mn} - \lg a_{MnO} - \lg K_6) = 0 \tag{37}$$

Newton iteration method is applied to solve eq. (33) or eq. (37), which are both nonlinear equations, and the obtained saturated solubility of oxygen is shown in Table 2. Equation (5) is used to calculate the saturated solubility of oxygen when the molar ratio X_{Si} is larger than 0.3, while in eq. (6) the case of X_{Si} is less than 0.1. For the oxide slags with X_{Si} ranging from 0.1 to 0.3, both eqs (5) and (6) can be used for the calculation.

Based on the above calculations, the saturated solubility of oxygen in Mn–Si melts is determined to be 0.0236 mass % in pure manganese at 1,700 K, which increases with increasing silicon content over a range from 0.1 to 0.3. The maximum value of oxygen solubility

Table 2: Saturated solubility of oxygen as a function of silicon content in Mn–Si melts at 1,700 K.

x_{Si}	[% Si]	M_{Mn-Si}	$\gamma_{O(Mn-Si)}^\circ$	$\Delta_{sol}G_O^\circ$ (J/mol)	$e_{O(Mn-Si)}^O$	$[\%O]_{(Mn-Si)}^{sat}$	
						From eq. (33)	From eq. (37)
0	0.00	54.94	1.56×10^{-5}	−204061	−0.2442	–	0.0236
0.1	5.38	52.26	1.20×10^{-5}	−208484	−0.2689	0.0342	0.0340
0.2	11.33	49.57	8.45×10^{-6}	−214207	−0.2937	0.0374	0.0370
0.3	17.97	46.89	5.70×10^{-6}	−220550	−0.3184	0.0429	0.0427
0.4	25.42	44.20	3.88×10^{-6}	−226834	−0.3432	0.0249	–
0.5	33.83	41.52	2.79×10^{-6}	−232383	−0.3679	0.0187	–
0.6	43.40	38.83	2.22×10^{-6}	−236520	−0.3927	0.0172	–
0.7	54.40	36.15	2.07×10^{-6}	−238570	−0.4174	0.0157	–
0.8	67.16	33.46	2.35×10^{-6}	−237859	−0.4422	0.0129	–
0.9	82.15	30.78	3.42×10^{-6}	−233718	−0.4669	0.0084	–
1	100.00	28.09	6.72×10^{-6}	−225480	−0.4917	0.0041	–

is 0.0427 mass % at X_{Si} 0.3 (17.97 mass %). The saturated solubility of oxygen decreases as the silicon content increases when the X_{Si} exceeds 0.3. It is determined that the saturated solubility of oxygen monotonously increases with X_{Si} over the range from 0 to 0.1. This will be discussed in detail in Section 4.2. The saturated solubility curve of oxygen in Mn–Si melts at 1,700 K is shown in Figure 1.

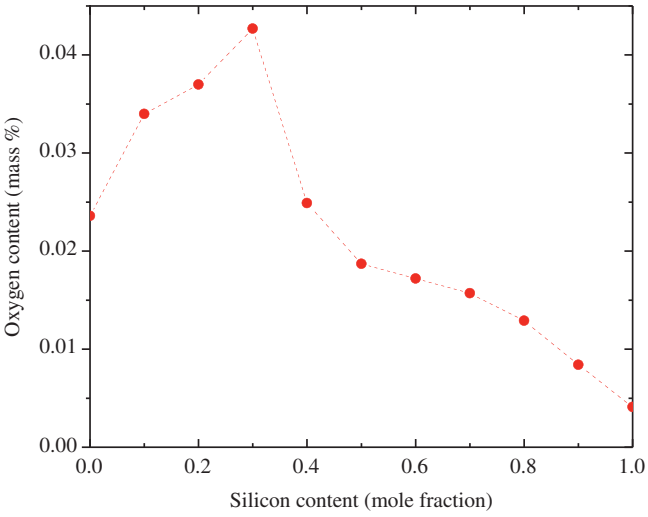

Figure 1: Saturated solubility of oxygen as a function of Si content in Mn–Si melts at 1,700 K.

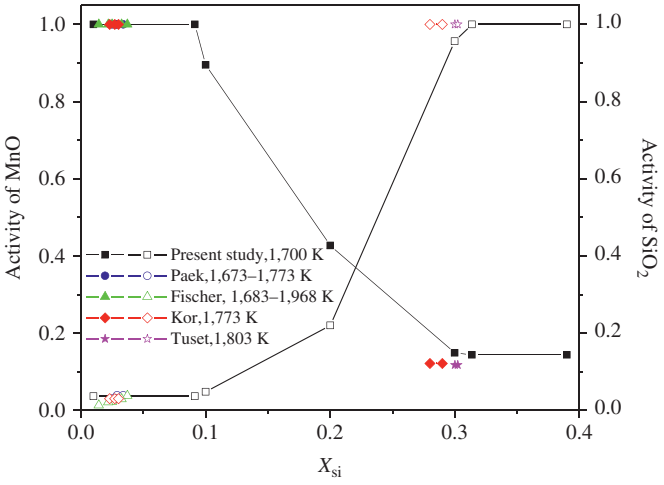

Figure 2: Effect of Si content on the activities of MnO and SiO_2 in oxide slags in equilibrium with Mn–Si melts at 1,700 K (reference state: MnO(s), SiO_2(s, tridymite)).

Discussion

The effect of silicon content on oxide inclusions in manganese ferroalloys

Figure 2 shows the effect of Si content on the activities of MnO and SiO_2 in oxide phases in equilibrium with Mn–Si melts at 1,700 K. In Figure 2, the solid and the open denote the activities of MnO and SiO_2, respectively. It could be seen that the activities of MnO and SiO_2 calculated in the present study are similar to the works of Fischer et al. [30], Kor [31], Paek et al. [32] and Tuset et al. [40].

When the molar ratio X_{Si} is 0.3 (corresponding to 18 mass %) in the Mn–Si melts, the equilibrium oxide phase with Mn–Si melts is a single liquid phase, which is composed of about 52.65 mass % MnO and 47.35 mass % SiO_2. The composition of its liquid oxide is just located near the liquid lines between liquid and solid SiO_2 on the phase diagram. In the Fe–Mn–Si ternary system, when the content of silicon is constant, the activity of Si increases with the increasing content of Fe [41]. The activities of silicon and manganese are greater than 0.0052 and less than 0.2852, respectively, in SiMn with the composition of 68 mass % Mn and 18 mass % Si (Mn68Si18Fe) at 1,700 K. The content of FeO in the FeO–MnO–SiO_2 ternary system in equilibrium with Fe–Mn–Si melts is negligible, when the contents of Mn and Si are high [41]. It is reasonable to assume that the oxide phase in equilibrium with SiMn at 1,700 K consists of MnO and SiO_2 according to Ref. [41] and the work of Fischer and Bardenheuer [30]. The oxide phase in equilibrium with Mn68Si18Fe melt is liquid phase saturated with solid SiO_2. Therefore, endogenous oxide inclusions mainly consist of SiO_2 and manganese silicate in SiMn containing 18 mass % Si. This is in good agreement with the Guo's work [13]. However, Bi et al. [14] reported that the main inclusions were REM oxides with some amounts of Si and Mn. The presence of REM oxides in the slags is attributed to REM in SiMn as REMs have a stronger affinity with oxygen than Si (or Mn).

In MCFeMn and LCFeMn containing 80 mass % Mn and less than 1.0 mass % Si, the equilibrium liquid oxide phase is saturated with solid MnO and have SiO_2 according to Ref. [41]. Therefore, the endogenous oxide inclusions are mainly MnO and also contain a small amount of tephroite in MCFeMn and LCFeMn, which is in good agreement with the work of Sjökvist et al. [11]. However, the works by Pande et al. [2] and Guo [13] reveal a different result, which may be related to the metallurgical process of the ferroalloys. The MCFeMn and LCFeMn

used in the works of Pande et al. [2] and Guo [13] were produced by the shaking ladle – electro-silicothermic process, in which the main reaction was the reduction of MnO by silicon. This chemical reduction may lead to a different composition of the slags.

The variation of saturated solubility of oxygen with the silicon content in the Mn–Si melts at 1,700 K

The equilibrium was established between the manganese melt containing silicon and the slag of CaO–SiO_2–MnO saturated with CaO at 1,823 K [17]. The saturated solubility of oxygen was 0.151–0.158 mass % in pure manganese, which was an order of magnitude higher than the experimental results in Refs [14, 16] and calculated results in Ref. [20] and current work. However, it was found that the oxygen solubility increased when the silicon content increased from 0.43 to 0.96 mass % (corresponding to X_{Si} ranging from 0.0084 to 0.0186).

Based on the work by Cheng [17] and present calculation, it is determined that oxygen solubility increases monotonically with the silicon content in the melt over a range of 0–0.1. The activities of manganese and silicon show strong negative deviations from ideality. When the X_{Si} is less than 0.1, the activity of manganese drops sharply and the activity of silicon is far low with the addition of silicon into the liquid manganese. It results in an increased oxygen solubility monotonically with the amount of silicon additions.

The limitation of the criteria for the minimum in terms of first-order activity interaction parameters

Oxygen solubility in Fe–Si melts equilibrium with silica at 1,873 K is much smaller than that in Mn–Si melts at 1,700 K with the same silicon content in the X_{Si} range from 0 to 0.8 as shown in Figure 3 [23]. One possible reason is that the silicon has a stronger affinity with manganese than iron. The activity of silicon in Fe–Si melts is much larger than that in Mn–Si melts at the same silicon content, while the activity of silicon in Fe–Mn–Si melts is between that of Fe–Si and Mn–Si melts. Thus, the saturated solubility of oxygen in Mn68Si18Fe is in the range from 1.5 [23] to 427 ppm at 1,700 K. However, the total oxygen content is about 800 ppm in SiMn products containing 18 mass % Si [13],

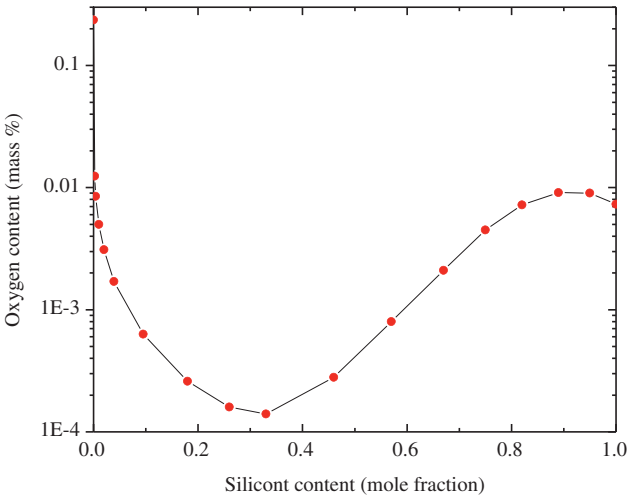

Figure 3: Oxygen solubility as a function of silicon content in Fe–Si melts equilibrium with silica at 1,873 K.
Reproduced from Ref. [23].

which is much larger than the oxygen solubility, leading to the formation of oxide inclusions in SiMn.

Conclusions

Calculations were carried out to predict the composition of oxide phases in equilibrium with Mn–Si melts at 1,700 K and the saturated solubility of oxygen in Mn–Si melts over a wide composition range. The following conclusions were obtained:

(1) The oxide phase was liquid phase saturated with solid MnO when the molar ratio X_{Si} is less than 0.1, while the oxide phase is liquid phase saturated with solid SiO_2 in the case of X_{Si} is greater than 0.3. But only a single liquid phase is equilibrated with Mn–Si melts in the X_{Si} range of 0.1–0.3. It is concluded that oxide inclusions mainly consisted of SiO_2 and manganese silicate in SiMn containing 18 mass % Si, and they were MnO and little tephroite for MCFeMn and LCFeMn with silicon content less than 1 mass %.

(2) Based on a subregular solution model, the saturated solubility of oxygen in Mn–Si melts was determined by the present work. The oxygen solubility is 0.0236 mass % in pure manganese at 1,700 K and increases as the silicon content increases over the X_{Si} range from 0.1 to 0.3. The maximum value of oxygen solubility of 0.0427 mass % occurred at the X_{Si} of 0.3 (17.97 mass %). Further increases in the silicon content will lead to a decreased saturated solubility of oxygen, and the minimum value , 0.0041 mass%, occurred in pure silicon.

Funding: The authors gratefully acknowledge research funding from the National Natural Science Foundation of China (no. 51274030) and Science Foundation for China Postdoctoral (no. 2012M520167).

References

[1] P.G. Jönsson, T. Sjöqvist and Ö. Grong, Proc. 9th Int. Ferroalloys Congr., Quebec (2001), 573–585.
[2] M.M. Pande, M. Guo, X. Guo, D. Geysen, S. Devisscher, B. Blanpain and P. Wollants, Ironmak. Steelmak., 37 (2010) 502–511.
[3] L. Holappa and S. Louhenkilpi, Proc. 13th Int. Ferroalloys Congr., Almaty (2013), pp. 1083–1090.
[4] M. Subramanian and C.N. Harman, Tool Alloy Steels, 23 (1989) 271–377.
[5] S.P. Srivastaava, S.N. Sinha, J.N. Bhambry and S.G. Tudekar, Proceedings of the Seminar on Problems and Prospects of Ferroalloy Industry in India, NML, Jamshedpur (1983), 299–308.
[6] O. Wijk and V. Brabie, ISIJ Int., 36 (1996) S132–S135.
[7] K.V. Grigorovich, S.S. Shibaev and I.V. Kostenko, Proc. 12th Int. Ferroalloys Congr., Helsinki (2010), 929–934.
[8] M.I. Gasik, A.I. Panchenko and A.S. Salnikov, Metall. Min. Ind., 3 (2011) 1–9.
[9] T. Sjökvist and P.G. Jönsson, Proc. 57th Electric Furnace Conf., ISS AIME, Pittsburgh, PA (1999), 383–393.
[10] T. Sjökvist, M. Göransson, P.G. Jönsson and P. Cowx, Ironmak. Steelmak., 30 (2003) 73–80.
[11] T. Sjökvist, P.G. Jönsson and Ö. Grong, Metall. Mater. Trans. A, 32A (2001) 1049–1056.
[12] P.W. Han, S.J. Chu, P. Mei and Y.F. Lin, J. Iron Steel Res. Int., 21 (2014) S23–S27.
[13] D.H. Guo, Ma.D. Thesis, University of Science and Technology Beijing, China (2011).
[14] Y.Y. Bi, A. Karasev and P.G. Jönsson, Steel Research Int., 85 (2014) 659–669.
[15] K.T. Jacob, Metall. Mater. Trans. B., 12B (1981) 675–678.
[16] V.H. Schenck, M.G. Frohberg and R. Nünnighhoff, Arch. Eisenhüttenwes., 35 (1964) 269–277.
[17] W. Cheng, Ph.D. Thesis, University of Science and Technology Beijing, China (1991).
[18] T. Narushima, K. Matsuzawa, Y. Mukai and Y. Iguchi, Mater. Trans. JIM., 35 (1994) 522–528.
[19] O.S. Klevan and T.A. Engh, Proc. 7th Int. Ferroalloys Congr., 1995. The Ferroalloys Association, Trondheim (1995), pp. 441–451.
[20] Y.N. Pivovarov and V.Y. Dashevskii, Russ. Metall., 2006 (2006) 286–290.
[21] J.P. Hajra, M. Wang and M.G. Frohberg, Z. Metallkde., 81 (1990) 255–260.
[22] M.G. Frohberg and M. Wang, Z. Metallkde., 81 (1990) 513–518.
[23] S.S. Shibaev, P.V. Krasovsku and K.V. Grigoravitch, ISIJ Int., 45 (2005) 1243–1247.
[24] V.Y. Dashevskii, A.M. Katsnelson, N.N. Makarova, K.V. Grigorovitch and V.I. Kashin, ISIJ Int., 43 (2003) 1487–1494.
[25] A. Tanaka, Trans. JIM., 20 (1979) 516–522.
[26] R. Gee and T. Rosenqvist, Scand. J. Metall., 5 (1976) 57–62.
[27] N. Ahmad and J.N. Pratt, Metall. Trans. A, 9A (1978) 1857–1863.
[28] A.I. Zaitsev, M.A. Zemchenko and B.M. Mogutnov, Rasplavy, 2 (1989) 9–19.
[29] G.I. Batalin and V.S. Sudavtsova, Inorg. Mater., 11 (1975) 1527–1531.
[30] W.A. Fischer and P.W. Bardenheuer, Arch. Eisenhüttenwes., 39 (1968) 559–570.
[31] G.J.W. Kor, Metall. Trans. B, 10B (1979) 367–374.
[32] M.K. Paek, J.M. Jang, Y.B. Kang and J.J. Pak, Korean J. Met. Mater., 50 (2012) 116–121.
[33] G.K. Sigworth and J.F. Elliott, Met. Sci., 8 (1974) 298–310.
[34] S.L. Wu, Ma.D. Thesis, University of Science and Technology Beijing, China (1986).
[35] C.H.P. Lupis and J.F. Elliott, Trans. TMS-AIME., 233 (1965) 257–258.
[36] K.P. Abraham, M.W. Davies and F.D. Richardson, J. Iron Steel Inst., 196 (1960) 82–89.
[37] S.R. Mehta and F.D. Richardson, J. Iron Steel Inst., 203 (1965) 524–528.
[38] B.K.D.P. Rao and D.R. Gaskell, Metall. Trans. B, 12B (1981) 311–317.
[39] D.R. Gaskell, Metall. Trans., 5 (1974) 776–778.
[40] J.K. Tuset, J. Sandvik and K. Venas, SINTEF Report III B0513 3892 34042, SINTEF, Trondheim, Norway (1971).
[41] J.X. Chen, Steelmaking Common Chart and Data Manual, Metallurgical Industry Press, Beijing (1984).